AD-A048 199   NIELSEN ENGINEERING AND RESEARCH INC MOUNTAIN VIEW CALIF   F/G 20/4
TESTING OF TURBULENCE MODELS BY EXACT NUMERICAL SOLUTION OF THE--ETC(U)
NOV 77   J H FERZIGER, O J MCMILLAN   N00014-77-C-0008

UNCLASSIFIED   NEAR-TR-155   NL

1 OF 1
ADA048 199

END
DATE
FILMED
1-78
DDC

FG.

12

NIELSEN ENGINEERING AND RESEARCH, INC.

OFFICES: 510 CLYDE AVENUE / MOUNTAIN VIEW, CALIFORNIA 94043 / TELEPHONE (415) 968-9457

COPY NO. 10

6 TESTING OF TURBULENCE MODELS BY EXACT NUMERICAL SOLUTION OF THE NAVIER-STOKES EQUATIONS,

by Joel H. Ferziger and Oden J. McMillan

10

14 NEAR-TR-155

11 4 November 1977

12 48p.

15 Contract N00014-77-C-0008
ONR Task NR 061-244

9 Annual Technical Report for Period
1 November 1976 -- 31 October 1977

NIELSEN ENGINEERING & RESEARCH, INC.
510 Clyde Avenue, Mountain View, CA 94043
Telephone (415) 968-9457

unclassified

SECURITY CLASSIFICATION OF THIS PAGE (*When Data Entered*)

REPORT DOCUMENTATION PAGE

READ INSTRUCTIONS BEFORE COMPLETING FORM

1. REPORT NUMBER	2. GOVT ACCESSION NO.
3. RECIPIENT'S CATALOG NUMBER	
4. TITLE (*and Subtitle*) TESTING OF TURBULENCE MODELS BY EXACT NUMERICAL SOLUTION OF THE NAVIER-STOKES EQUATIONS	5. TYPE OF REPORT & PERIOD COVERED Technical Report 11/1/76 - 10/31/77
	6. PERFORMING ORG. REPORT NUMBER NEAR TR 155
7. AUTHOR(s) Joel H. Ferziger and Oden J. McMillan	8. CONTRACT OR GRANT NUMBER(s) N00014-77-C-0008 NEW
9. PERFORMING ORGANIZATION NAME AND ADDRESS Nielsen Engineering & Research, Inc. 510 Clyde Avenue Mountain View, CA 94043	10. PROGRAM ELEMENT, PROJECT, TASK AREA & WORK UNIT NUMBERS NR 061-244
11. CONTROLLING OFFICE NAME AND ADDRESS Office of Naval Research Code 430B, Department of the Navy Arlington, VA 22217	12. REPORT DATE 4 November 1977
	13. NUMBER OF PAGES 47
14. MONITORING AGENCY NAME & ADDRESS (*if different from Controlling Office*)	15. SECURITY CLASS. (*of this report*) Unclassified
	15a. DECLASSIFICATION/DOWNGRADING SCHEDULE NA

16. DISTRIBUTION STATEMENT (*of this Report*)

Approved for public release; distribution unlimited.

17. DISTRIBUTION STATEMENT (*of the abstract entered in Block 20, if different from R...*)

NA

18. SUPPLEMENTARY NOTES

19. KEY WORDS (*Continue on reverse side if necessary and identify by block number*)

Turbulence
Mathematical Models
Eddies

20. ABSTRACT (*Continue on reverse side if necessary and identify by block number*)

This report presents preliminary results from a continuing study in which the validity of models used in large-eddy simulations of turbulent flow is tested by comparison with results from an exact simulation using the Navier-Stokes equations. The results to date are for models of the eddy-viscosity type applied to a homogeneous isotropic incompressible flow. More complicated flows and models will be considered in future phases of this study.

DD FORM 1 JAN 73 1473 EDITION OF 1 NOV 65 IS OBSOLETE

Unclassified

SECURITY CLASSIFICATION OF THIS PAGE (*When Data Entered*)

PREFACE

This technical report covers the work performed under Contract N00014-77-C-0008 from 1 November 1976 to 31 October 1977, and is the first report published under the program. The program is sponsored by the Office of Naval Research with significant assistance provided by NASA/Ames Research Center.

Mr. Morton Cooper, Office of Naval Research, is the Navy Scientific Officer. Dr. Robert S. Rogallo is the NASA advisor.

TABLE OF CONTENTS

INTRODUCTION

Under the sponsorship of the Office of Naval Research (ONR), Nielsen Engineering & Research, Inc. (NEAR) is conducting a program the objective of which is the testing of turbulence models using the most accurate methods of computing turbulent flows now available. In order to limit the number of possible sources of discrepancy between the predictions of a model and the results of an accurate computation, the program has begun by looking at the simplest turbulent flows and the simplest models. Since the program is expected to continue for a few years, it has been designed so that new features (geometric complexity and/or physical phenomena) will be added one at a time. This should provide an expanding base of confidence to build on and will, we hope, avoid some of the difficulties that other researchers have had in sorting out various effects in turbulent flows and in learning to model them.

There are two distinct levels of turbulent flow computation for which models will be investigated. When the time-averaged Navier-Stokes equations are used to describe a flow, the Reynolds stresses, which are essentially the averages of products of the fluctuating components of the velocity, need to be modeled. In large-eddy simulation, on the other hand, averages of the products of the small-scale components occur and require modeling. By analogy, these are called the subgrid-scale Reynolds stresses but they represent a different set of physical phenomena than the time-average Reynolds stresses. However, it is believed that both sets of quantities can be modeled in similar ways.

The basic approach to model validation used is to compute an accurate estimate of the quantity to be modeled and, simultaneously, the value that the model would predict for the same quantity. Comparison, usually by means of a correlation coefficient, then provides the information as to the validity of the model; constants in a model can also be evaluated. This general approach could be implemented in several ways. In the first, exact Navier-Stokes simulations of turbulent flows could be used to validate both subgrid-scale and time-average models. The difficulty is that only a few turbulent flows (all at low Reynolds number) are accessible to exact simulation and this severely restricts what can be done in terms of time-average model testing. In another possible implementation, large-eddy simulations could be used to test time-average models; the problem here is that the effects of the subgrid-scale turbulence (which has to be modeled in the large-eddy simulation) may be difficult to estimate.

Since it is the implementation of the basic approach that provides the best accuracy, we have chosen to begin by using exact Navier-Stokes simulations to test subgrid-scale models. We believe that this is the area in which the most information can be generated in the shortest time. One can also argue that the same models ought to be good for both kinds of modeling and we are therefore indirectly generating information about time-average modeling. Of course, the last statement needs to be checked carefully and this will be done in later stages of the program.

The exact simulations that we are using as the basis for the model checking are provided by Dr. Robert Rogallo of NASA/Ames Research Center. NASA has also made their computer available to this program at no cost. To date, the only flow field that has been available to us has been a simulation of the decay of homogeneous isotropic turbulence. We have used these data as input to a computer code that we have written to process the data and do the necessary correlations. As an initial test of both the input data and our code, we compare our results with those of Clark, et al. (ref. 1). The results of these tests are given in this report and, although a few further checks are necessary, they have shown that both Rogallo's code and ours seem to be working satisfactorily. Extensions of this work are currently underway.

The next section of this report contains a description of the computer code developed by NEAR. The third section presents the results we have generated to date, and the last section describes extensions of this work to be undertaken in succeeding contract years.

THE NEAR COMPUTER CODE

Description

The spectral simulation of the Navier-Stokes equations developed by R. S. Rogallo (ref. 2) on the ILLIAC IV at the NASA/Ames Research Center results in values for the three velocity components u_i at each point in a 64^3 grid at each time step in the calculated evolution of a homogeneous incompressible flow. If the Taylor-microscale Reynolds number (R_λ) of the flow being simulated is less than about 40, this grid is fine enough to capture essentially all of the energy and dissipation in the flow, and these results can be considered "exact".

Imagine that the same homogeneous incompressible flow is to be calculated on a coarser grid using a large-eddy simulation. The equation set to be solved is

$$\left.\begin{aligned} &\frac{\partial \bar{u}_i}{\partial x_i} = 0 \\ &\frac{\partial \bar{u}_i}{\partial t} + \frac{\partial}{\partial x_j}\left(\overline{\bar{u}_i \bar{u}_j}\right) = -\frac{\partial P}{\partial x_i} + \nu \nabla^2 \bar{u}_i - \frac{\partial}{\partial x_j}\left(\tau_{ij} + C_{ij}\right) \end{aligned}\right\} \quad (1)$$

where the overbar denotes a spatially filtered variable

$$\bar{f}(\underline{x}) \triangleq \int G(\underline{x}-\underline{x}')f(\underline{x}')d\underline{x}', \quad (2)$$

$G(\underline{x})$ is the selected spatial filter function, $f(\underline{x})$ is any field variable, and the indicated integration is over all space. The underscore denotes a vector quantity. Also in equation set (1),

$$\left.\begin{aligned} u_i' &= u_i - \bar{u}_i \\ P &= \bar{p}/\rho + 1/3\left(\overline{u_k' u_k'} + 2\overline{\bar{u}_k u_k'}\right) \\ \tau_{ij} &= \overline{u_i' u_j'} - 1/3\, \overline{u_k' u_k'} \\ \text{and} \quad C_{ij} &= \overline{\bar{u}_i u_j'} + \overline{u_i' \bar{u}_j} - 2/3\left(\overline{\bar{u}_k u_k'}\right) \end{aligned}\right\} \quad (3)$$

The solution variables in these equations are $\bar{u}_i$ and P; the terms involving finer scales than are resolvable on the coarse mesh of the LES (i.e., those involving τ_{ij} and C_{ij}) must be modeled in terms of $\bar{u}_i$.

The object of our work, as previously stated, is to evaluate models of the type used in large-eddy simulations. Our evaluation is of several eddy-viscosity models for τ_{ij} (for a model for C_{ij} and its evaluation, see ref. 1). Because in large-eddy simulations models constructed for τ_{ij} are often used to approximate the combination $\tau_{ij} + C_{ij}$, we also evaluate how accurately these same models represent this quantity. The methodology used to conduct this evaluation is in general terms as follows. Rogallo's code is used to generate the velocity field u_i on a 64^3 grid (with grid spacing Δ) at a specified time step in the evolution of a selected homogeneous, *incompressible flow*. For a selected filter function $G(\underline{x})$ (a three-dimensional Gaussian with filtering length scale $\Delta_a = 8\Delta$ is the initial choice in this work), exact values are calculated for $\bar{u}_i$, u_i' and τ_{ij} on the 64^3 grid using relations (2) and (3) and this u_i field.* Values of $\partial\tau_{ij}/\partial x_j$ are calculated on the 64^3 grid. A coarse grid (16^3, with spacing $\Delta_c = 4\Delta$, thus $\Delta_a/\Delta_c = 2$) representing that used in a hypothetical LES of the same flow is overlaid on the 64^3 grid. Exact values of $\bar{u}_i$, τ_{ij} and $\partial\tau_{ij}/\partial x_j$ on the coarse grid are extracted from the 64^3 grid. Using these fields, exact values of $\bar{u}_i\ \partial\tau_{ij}/\ x_j$ are calculated on the coarse grid. Models (M_{ij}) for τ_{ij} in terms of $\bar{u}_i$ are also calculated on the coarse grid, as are values of $\partial M_{ij}/\partial x_j$ and $\bar{u}_i\ \partial M_{ij}/\partial x_j$. The derivatives required for the model calculations are done using any one of several numerical schemes. At this point, we possess (on the coarse grid) both exact and modeled values of the subgrid-scale stress (τ_{ij} and M_{ij}), the divergence of this stress ($\partial\tau_{ij}/\partial x_j$ and $\partial M_{ij}/\partial x_j$), and the energy dissipation by this stress ($\bar{u}_i\ \partial\tau_{ij}/\partial x_j$ and $\bar{u}_i\ \partial M_{ij}/\partial x_j$).

---

*For the case where $\tau_{ij} + C_{ij}$ is being modeled, substitute $\tau_{ij} + C_{ij}$ for τ_{ij} in this description.

The assessment of the validity of the models used can now proceed on three levels as was pointed out by Clark (ref. 1): (1) the tensor level, where models (M_{ij}) are compared directly to the exact subgrid-scale stress (τ_{ij}); (2) the vector level, where $\partial M_{ij}/\partial x_j$ is compared to $\partial \tau_{ij}/\partial x_j$; and (3) the scalar level, where $\bar{u}_i \; \partial M_{ij}/\partial x_j$ is compared to $\bar{u}_i \; \partial \tau_{ij}/\partial x_j$. At each of these levels, the comparison is done by means of calculating correlation coefficients

$$C(M,X) = \frac{\langle MX \rangle}{\langle M^2 \rangle^{1/2} \langle X^2 \rangle^{1/2}} \tag{4}$$

where $\langle \; \rangle \triangleq \frac{1}{16^3} \sum_{16^3} (\;)$, $M \triangleq$ model value, $X \triangleq$ exact value. The magnitude $|C(M,X)|$ will vary between 0 (if M and X are totally unrelated) to 1 (if the model is exact to within a multiplicative constant). Notice that at the tensor level, a correlation coefficient is calculated for each stress component (6 of which are independent); the arithmetic average of these coefficients gives a sense of the correlation for the whole tensor. Similarly, at the vector level, there are three correlation coefficients (and their average), and at the scalar level, one correlation coefficient.

These correlation coefficients are independent of the value used for the constant in a given model. Values for the constants can be determined, however, by forcing agreement of the root mean* square (RMS) modeled and exact values. At the tensor level, a separate value of the constant can be obtained in this way for the diagonal and off-diagonal components; another value of the tensor-level constant can be derived by applying this RMS criterion to the sum of squares of the stress components at each grid point. Similarly, three values for the constant (and an "overall" value) are available at the vector level, and one at the scalar level.

---

*On the 16^3 mesh

The models evaluated are all of the eddy-viscosity type:

$$\left.\begin{aligned} M_{ij} &= \alpha_{ij} - 1/3\ \alpha_{kk}\delta_{ij} \\ \alpha_{ij} &= 2K\bar{S}_{ij} \\ \bar{S}_{ij} &= 1/2\left(\frac{\partial \bar{u}_i}{\partial x_j} + \frac{\partial \bar{u}_j}{\partial x_i}\right) \end{aligned}\right\} \qquad (5)$$

The models are:

1. The Smagorinsky Model, $K = (C_s\Delta_a)^2[2\bar{S}_{ij}\bar{S}_{ij}]^{1/2}$, where Δ_a is the averaging length scale, and C_s is the model constant.

2. The Vorticity Model, $K = (C_v\Delta_a)^2(\bar{\omega}_i\bar{\omega}_i)^{1/2}$, where C_v is the model constant and $\bar{\omega}_i = \varepsilon_{ijk}\ \partial\bar{u}_k/\partial x_j$.

3. The Kinetic Energy Model, $K = (C_q\Delta_a/3)(\overline{u_k'u_k'})^{1/2}$, where C_q is the model constant and $1/3\ \overline{u_k'u_k'}$ is the exact subgrid-scale kinetic energy.

4. The constant-eddy-viscosity model, $K = C_c$.

A program has been written for the CDC 7600 computer to accomplish the above tasks. Because even this computer cannot store in core a complete velocity field on a 64^3 grid, this program incorporates a considerable amount of data transfer to and from auxiliary disc memory. This data transfer results in lengthy residence time in computer input/output queues, although computation times are reasonable. Unfortunately, it is usual for any sophisticated computer system to "crash" quite frequently, and it so happens that the mean time between crashes for the CDC 7600 is less than the residence time to complete the analysis of a time step for a given flow field. It was necessary therefore to divide the program up into ten subprograms, each with restart capability in the event of a system failure during execution. These subprograms are run sequentially and are named CALCIA, CALCIB, CALCIC, CALCII, CALCIII, CALCIV, CALCV, CALCVI, CALCVII and INCORE. A description of these subprograms and the major subroutines used can be found in the Appendix. This section is concluded with a brief discussion of the means used to verify the accuracy of the results of these programs, and a discussion of the changes made to evaluate the same models as applied to $\tau_{ij} + C_{ij}$.

Checkout of the Computer Code

To debug these programs and verify their accuracy, they were used to analyze an analytically specified, artificial "flow field", the Taylor-Green flow field:

$$\left.\begin{aligned} u_1 &= \cos ax_1 \sin ax_2 \cos ax_3 \\ u_2 &= -\sin ax_1 \cos ax_2 \cos ax_3 \\ u_3 &= 0 \end{aligned}\right\} \qquad (6)$$

where $a = 2\pi/64$, x_i are in the domain [0,63]. Notice that this "flow field" satisfies continuity exactly, but does not, of course, have any features of turbulence. Its utility for checking out the code lies in its simplicity, its exact periodicity, and the fact that because of its wave number content, the quantities $\bar{u}_i$, τ_{ij}, $\partial\tau_{ij}/ x_j$, S_i, F_i, $\bar{S}_i$ and $\bar{F}_i$ can be calculated exactly by the CDC 7600 program and compared to simple closed-form expressions. Quantities used in the model calculations, although not calculated exactly on the 16^3 mesh, may also be compared to (more complicated) closed-form expressions to ensure that the code is operating correctly. These comparisons have been carried out on randomly selected elements of the appropriate mesh (64^3 or 16^3).

Notice that because $u_3 = 0$, $\tau_{13} = \tau_{31} = \tau_{23} = \tau_{32} = \bar{u}_3\, \partial\tau_{3j}/\partial x_j = 0$. Correct calculation of these zero elements does not guarantee that some problem is not being masked. Therefore, the Taylor-Green flow was analyzed twice more, each time after rotating the coordinate system to place the zeros in different elements.

Modifications to the Code to Apply the Same Models To $\tau_{ij} + C_{ij}$

This was simply accomplished by changing those portions of the code that do input/output on the 64^3 grid to include the appropriate elements of C_{ij}. A second version of the program set was prepared in which these changes were made.

RESULTS TO DATE

Since the approach to model validation adopted by this program requires the use of two large computer codes (one to calculate the field and a second to analyze the data and produce correlations), it was decided early on that the initial task should be the repetition, as closely as possible, of at least one case that has already been computed and analyzed. The only case available at the present is that of Clark, et al. (ref. 1). Clark simulated the 2.54 cm grid-turbulence experiment of Comte-Bellot and Corrsin (ref. 3) and, on obtaining good agreement with the experimental data, he used the computed results to test subgrid-scale models. We will present his results alongside ours below.

To facilitate the comparison, we wrote the computer code described in the previous section and requested Dr. Rogallo to run a simulation of the Comte-Bellot and Corrsin flow. His results were provided to us in the form of a tape which was used as the input to our program. Before going on to the results, it is important to compare Rogallo's simulation with Clark's. Both programs compute the flow field on a 64^3 grid. Clark's program used a fourth-order spatial finite-difference method while Rogallo's uses Fourier methods (in fact he treats the Fourier transform of the velocity as the basic dependent variable but that difference is not important). Clark used a third-order predictor-corrector scheme for the time advancement while Rogallo has chosen the fourth-order Runge-Kutta method. These differences are not expected to have a significant effect on the results. For ease of comparison in this report, time is expressed in terms of Clark's time steps; i.e., number of time steps = (time in seconds)/.0073.

The initial field for Rogallo's program was constructed in the same way as Clark's. However, in constructing the spectrum, Rogallo has used different subdivisions in wave number space than did Clark. As a result, Rogallo's spectra look lumpy even though they are in fact the same as Clark's, cf., Fig. 1. A more serious difficulty is that, due to an oversight, a viscosity was used that is twice as big as it ought to be and the Reynolds number is only about half of the desired value (see Fig. 2). Also, the time scale was incorrect for a similar reason. Consequently, the results obtained do not match the experimental energy decay or dissipation rate as well as they should; these results are shown in Figs. 3 and 4. Note that because of the incorrect time scaling, Rogallo's last time point is not the same as Clark's.

We now turn to results that were generated by our code. First we give some of the statistics of the flow field. The skewness of the velocity derivative is shown in Fig. 5 and the flatness is given in Fig. 6. In Fig. 5, we compare the skewness values obtained from each of the three velocity components with those of Clark. Clark provided the skewness for only one component of the velocity but has informed us privately that the other components show about the same scatter as the results we obtained. Our skewnesses tend to be a bit higher than his. This is probably due to the use of Fourier methods to obtain the velocity derivatives. Fourier methods differentiate more accurately, especially at high wave numbers, and the skewness is sensitive to the high-wave-number components of the velocity field. Similar remarks apply to the flatness but Clark did not report values of this quantity. We also note that skewness seems to rise to the equilibrium value more slowly in our calculation than in Clark's. The precise reason for this is not known but we would guess that it may be due to the high-wave-number portion of the field requiring more time to come to equilibrium than the low-wave-number part. Since our calculation of the skewness is more sensitive to the high-wave-number components, this might explain the relatively slow rise of the skewness. Also shown in Figs. 5 and 6 are the skewness and flatness of the filtered field. As expected, they are quite a bit below the values for the full field. We intend to further investigate the effect of filtering on the skewness and flatness in the near future. This would assist in the comparison of large-eddy simulations with experiment, cf., Ferziger, et al. (ref. 4). A preliminary look into this has not provided anything useful in this regard.

We now turn to results obtained from the filtered field. As explained in the previous section, Rogallo's velocity field was filtered by the use of Fourier methods using a Gaussian filter. Once the filtered field has been computed, we can obtain the subgrid-scale field by subtraction. From this point, we can go on to calculate the subgrid-scale Reynolds stresses, the derivatives of the filtered field and all of the quantities that go into a model. We have so far investigated only those models that were considered by Clark: the Smagorinsky model, the vorticity model, a one-equation subgrid-scale kinetic energy model, and a constant-eddy-viscosity model.

One measure of the overall accuracy of the calculations comes from comparing dissipation caused by the subgrid-scale Reynolds stresses. These are displayed in Fig. 7. The comparison with Clark's results is fairly good. The reason for the higher values at the early time steps in our calculation is not known and seems a little surprising in view of the fact that our field seems to come to equilibrium more slowly than Clark's.

Now we come to the detailed correlation results. As mentioned earlier, correlations can be done at three different levels. At the most detailed level, the subgrid-scale Reynolds stresses are compared with the model directly; Clark called this the tensor level. At the second level we note that it is only the divergence of the stress tensor that appears in the dynamical equations and we compare the divergence of the exact Reynolds stress with the divergence of the model; Clark termed this the vector level of comparison. At the crudest level we argue that the main function of the subgrid-scale model is to dissipate the kinetic energy of turbulence in the right amount and at the right places and we compare the energy dissipation of the exact result and the model prediction. This is done by taking the scalar product of the divergence with the velocity vector itself; Clark calls this the scalar level of comparison.

We thus have four different models that we wish to evaluate at three different levels. The comparison should also be made at several different time steps to check that the results are not peculiar to one particular field. (They ought to be checked on different realizations of the flow as well but the expense of generating flow fields has precluded this. A small amount of this kind of checking will be done in the future.) The question of whether there is a variation with time is easily disposed of. Figure 8 shows the results for the Smagorinsky model using a standard centered difference scheme to do the differentiation required in the model calculations, and it is seen that the variation with time is not significant. The results for the vorticity and constant-eddy-viscosity models are very similar and are not shown for this reason; the latter is a bit of a surprise. For the turbulent kinetic energy model, however, we find that the correlation coefficient is essentially constant but there is a small increase in the constant with time as shown in Fig. 9. This may have important implications for turbulence modeling but the result was only recently obtained and we have not had time to analyze it as yet. In view of the constancy of most of the results with time, we will concentrate on one time step from now on.

In Tables 1-4 the correlation coefficients are given for the four models at each of the three levels. There is no significant difference among the models as far as the correlation coefficients are concerned. In fact, at the tensor level the correlations are much closer when a given component is compared for the various models than when the individual components are compared for a particular model. This is consistent with Clark's results and probably means that the correlation is a property of eddy-viscosity models in general and has little to do with the particular form chosen for the eddy viscosity. If this is so (and, again, it is in agreement with Clark's results), it means that the prognosis for one- or two-equation subgrid-scale models is not good--a constant-eddy-viscosity model will do essentially as well as a more sophisticated model.

Or to put it another way, a more sophisticated model will do as badly as the constant-eddy-viscosity model. This result, important though it may be, requires further checking on other flows before it can be accepted as established. The generalization of this result to Reynolds-stress modeling is on even shakier ground but it suggests an important line of research that we intend to take as soon as the tools and the necessary data are available. The constants for each of the first three models (obtained by equating the RMS value of the model with the exact result) are given in Table 5.

In Table 6 are presented the correlation coefficients obtained using different methods of calculating the derivatives in the model calculations. The methods used are the standard centered difference formula (L = 1), a centered difference formula using more widely spaced points (L = 2), and the spectral method. It is seen that the correlation coefficients obtained from the standard centered difference formula and from the spectral method are essentially the same, while those from the alternate centered difference formula are lower. Use of a centered difference formula is approximately equivalent to using a "box" filter of width equal to the distance between the points at which the function is evaluated. Thus the use of difference formulas with different mesh spacing is a quick and easy (although non-exact) way to search for effects of averaging in the model calculations. It has been suggested by Leslie and coworkers (ref. 5) that subgrid-scale models are improved by averaging them over small regions of space; they suggested averaging over a region of characteristic length of about twice the width of the filter. Recent work of the Stanford group provides indirect confirmation of this. However, the results in Table 6 for L = 2 vs. L = 1 indicate that the correlation is not improved by averaging the model over more than one filter width. A more careful study of this will be undertaken in the near future.

Table 6 also compares our results with those of Clark. Clark used a fourth-order finite difference formula on his 8^3 coarse grid to do the model calculations. It is clear that our correlations (excluding those using L = 2) agree well with his at the tensor level but are smaller at the vector and scalar levels of comparison. In fact, the improvement that Clark found in going from the tensor to the vector level seems to be absent in our results. The reason for this is not understood at the present time but some of the studies to be made in the near future should shed light on this. That there are several possible causes of the discrepancies is clear upon examination of Table 7, which summarizes the parameters and methods used in the present work with those of Clark. Those differences thought to be important are:

1. Our calculations were made at a Reynolds number that is only about half of Clark's. It is possible that we are seeing a Reynolds number effect. Since the effect of Reynolds number is one of the highest priority items for the near future, this possibility will be checked out soon.

2. Rogallo's calculation used Fourier methods whereas Clark's used finite differences. It is possible that the two flow fields differ in the high wave number part of the velocity field. Since these contain most of the contribution to the subgrid-scale turbulence component, it is possible that the source of the difference lies here.

3. We used a Gaussian filter and Clark used a box filter. The effect of filter type on the results is a relatively easy item to check using the code we have developed. We will be looking not only at the two filters mentioned above (the Gaussian and the box) but also at a filter that corresponds to a sharp cutoff in Fourier space.

4. We used a finer "coarse" mesh than did Clark (16^3 vs. 8^3) to improve the accuracy of the numerical techniques used in the model calculations and to increase the sample size for our statistical evaluation process. After the other effects listed above are evaluated, this difference can be eliminated if it is warranted.

Table 8 compares our model constants obtained using the standard centered difference formula and the spectral method with those that Clark obtained. The model constants we calculated show more dependence on the method of differentiation used than the correlation coefficients did. With the exception of the kinetic-energy model, our values are lower than Clark's. We suspect that this may be due to the effects listed above, but it is impossible to be confident about this until the further checks mentioned above are made.

Finally, we note that although Clark did the kind of testing done above, some authors define the subgrid-scale Reynolds stress to be $\overline{u_i'u_j'} + \overline{\bar{u}_i u_j'} + \overline{u_i'\bar{u}_j}$ rather than $\overline{u_i'u_j'}$. We have therefore tested the models given above as models of this modified subgrid-scale Reynolds stress and the results are given in Table 9. It is clear that the models work better for the $\overline{u_i'u_j'}$ term than for the combined term. Again, this result may depend on the effects listed above.

FUTURE DIRECTIONS

As stated earlier, this work is only the beginning of a longer program. The computer code that was used to obtain the results of the previous section has been available for only a short time and the results given are definitely of a preliminary nature. Essentially, most of the first year of the program was spent in developing a tool which will be used in the future. The coming year should therefore see a considerable increase in the rate at which the work progresses. A possible bottleneck may be the fact that the data we analyze are obtained on the ILLIAC IV by other researchers and is not within the control of Nielsen Engineering and Research, Inc.

Some of the future directions were already stated. We will, in the near future, look at the effects mentioned in the previous section. Specifically, the effects of Reynolds number, filter type and filter length scale will be looked at. If necessary, we will also look at a further comparison of Clark's and Rogallo's fields.

The work will also be extended to consider flows other than decaying homogeneous turbulence. Specifically, we will look at homogeneous strained and sheared turbulence. We will also begin to look into the possibilities of full subgrid-scale Reynolds stress modeling, i.e., the possibility of treating the subgrid-scale stress by means of a set of six partial differential equations.

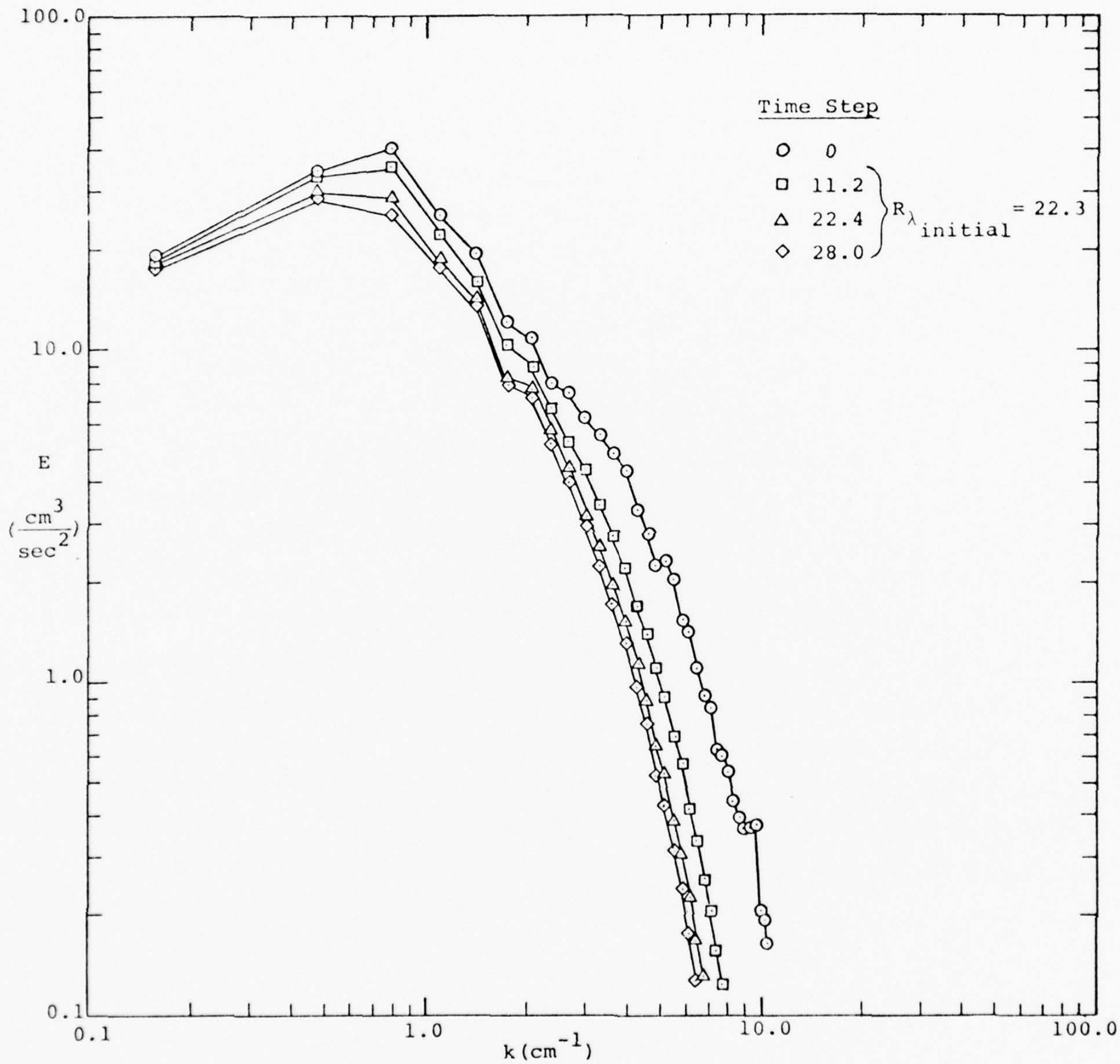

Figure 1. Energy spectrum as a function of time, Rogallo's simulation.

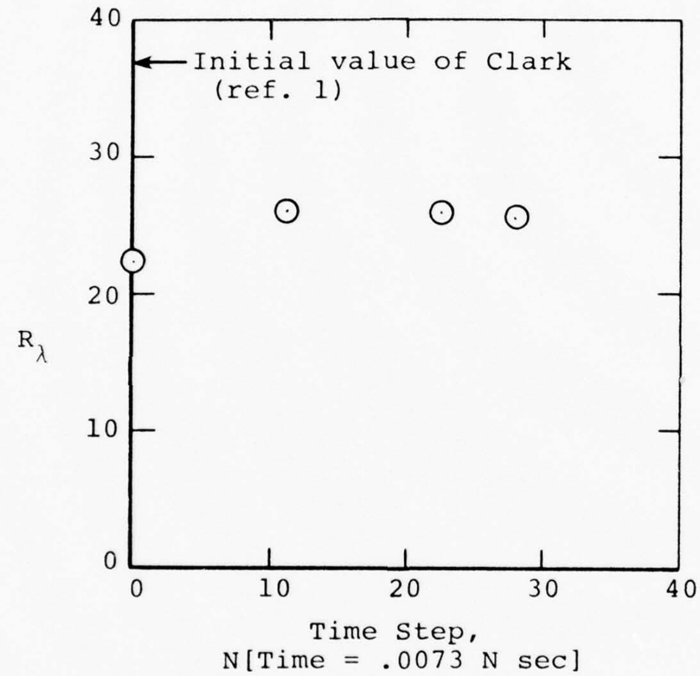

Figure 2. Reynolds number based on Taylor microscale as a function of time, Rogallo's simulation.

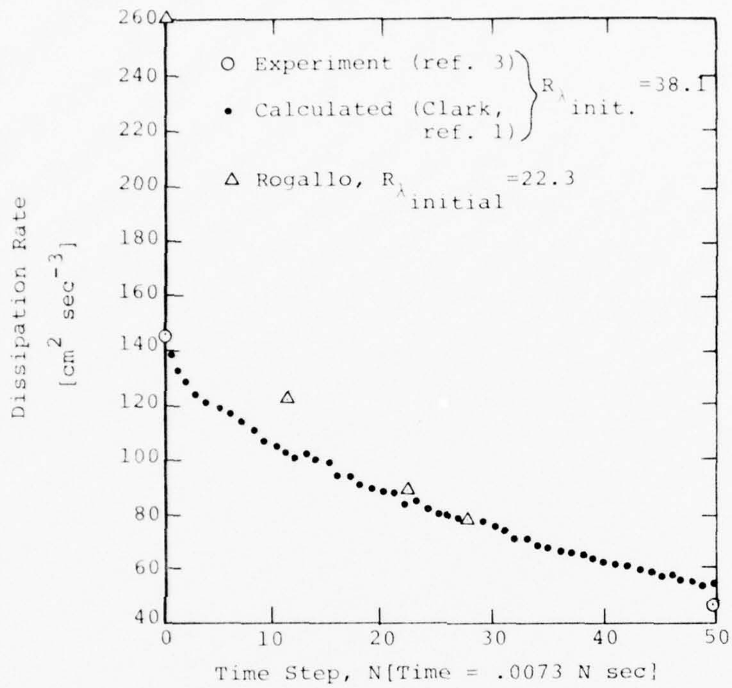

Figure 3. Dissipation rate as a function of time step. (Note shifted origin)

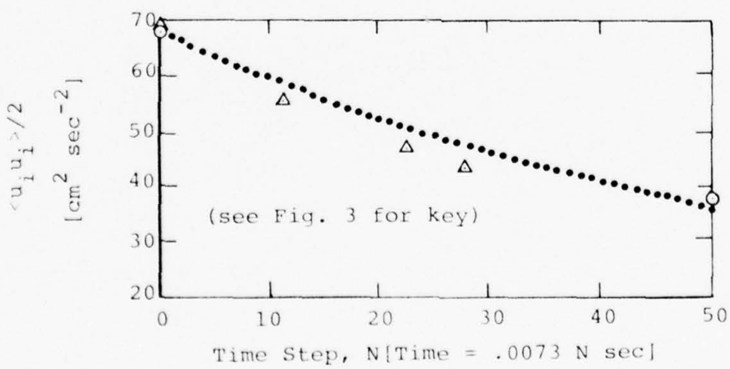

Figure 4. Energy as a function of time step. (Note shifted origin)

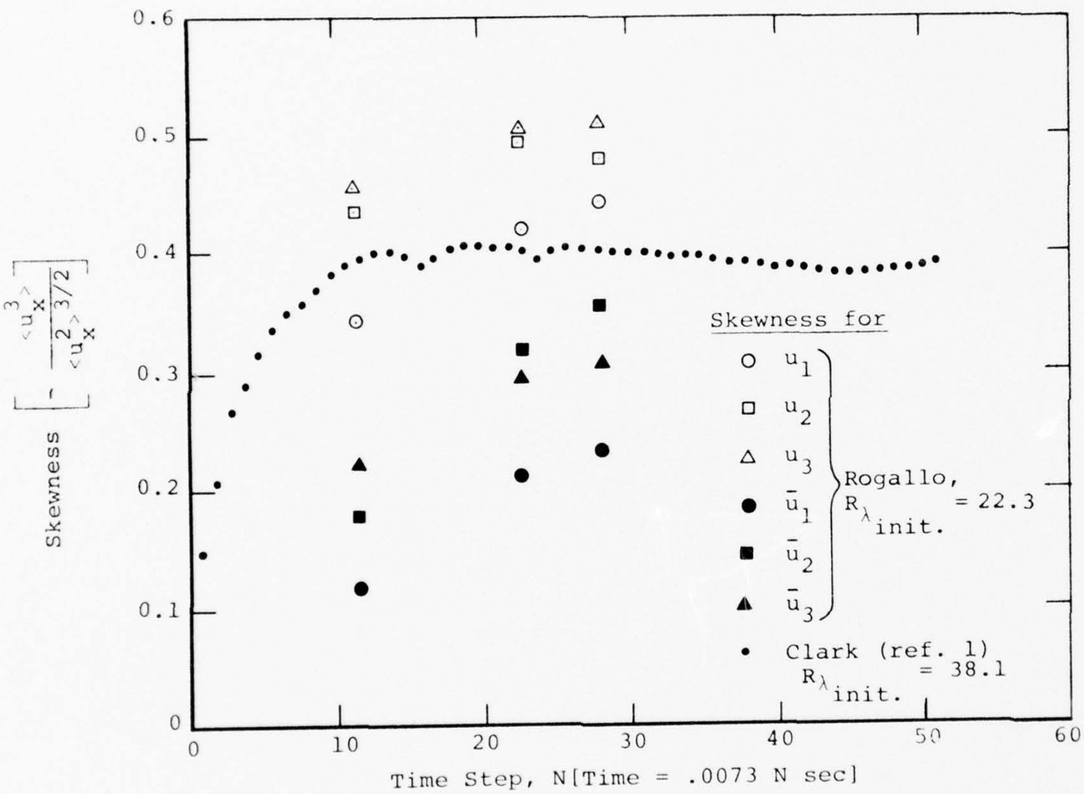

Figure 5. Skewness as a function of time.

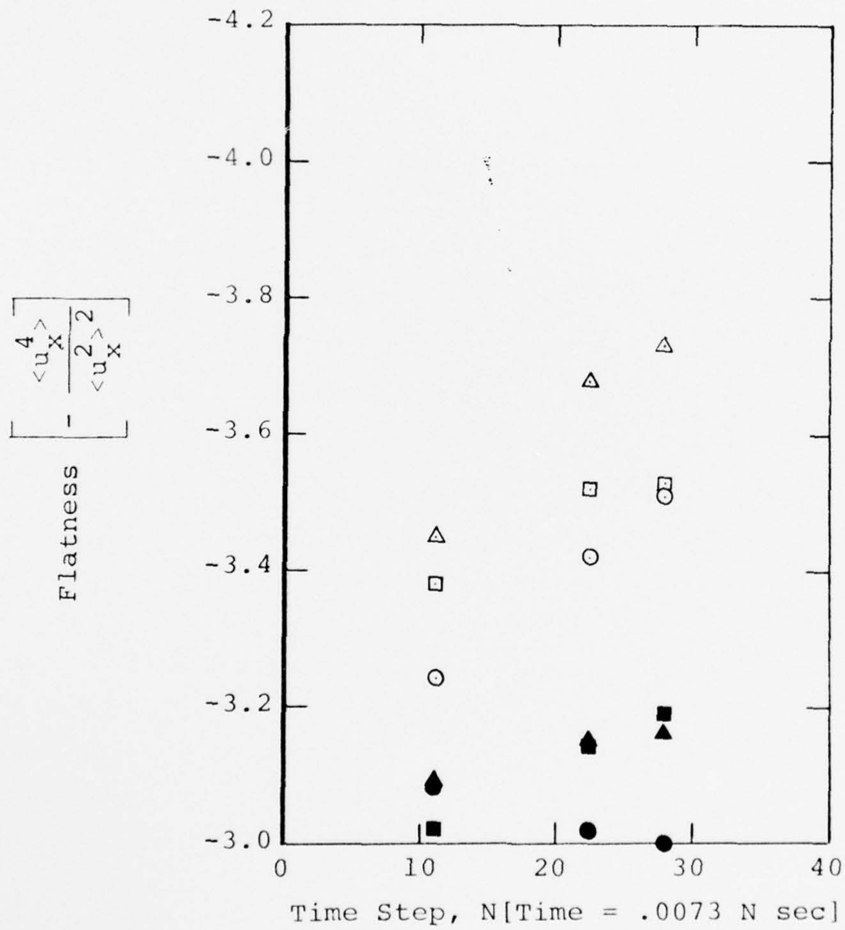

Figure 6. Flatness as a function of time (note shifted origin; for key see fig. 5).

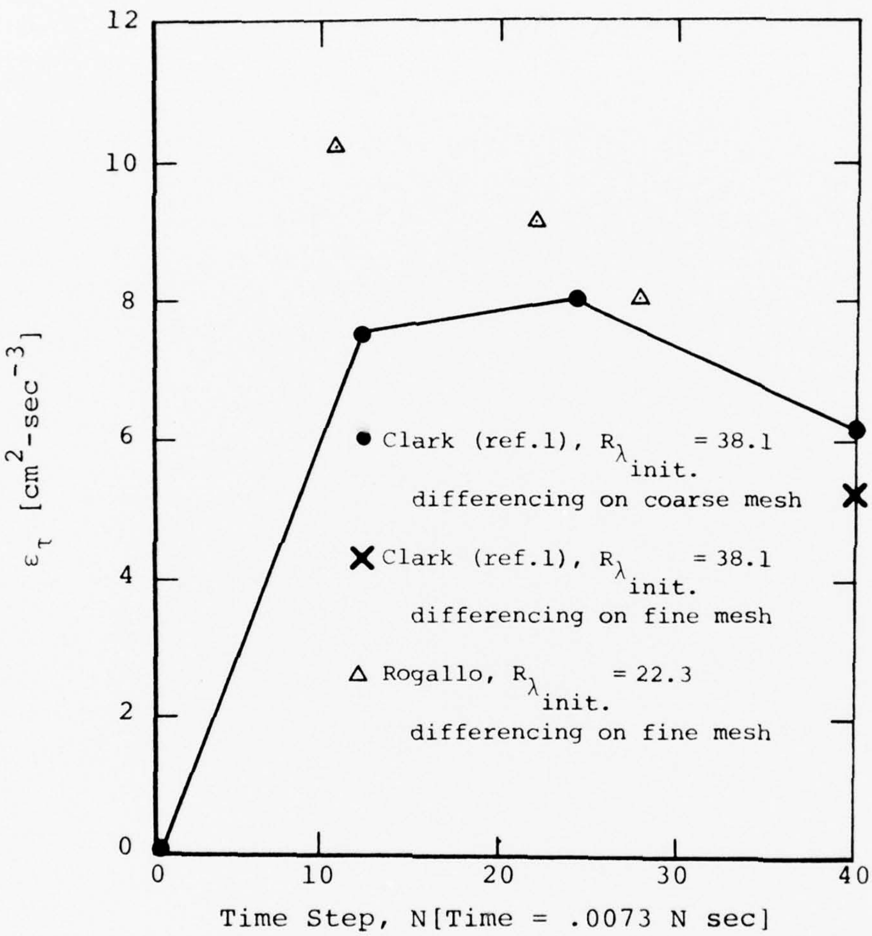

Figure 7. Subgrid-scale dissipation rate, ε_τ.

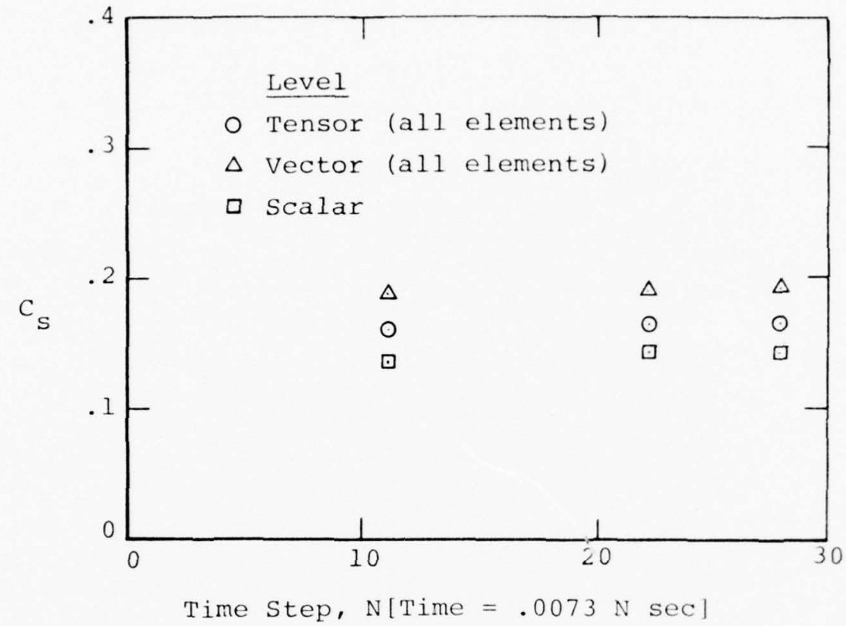

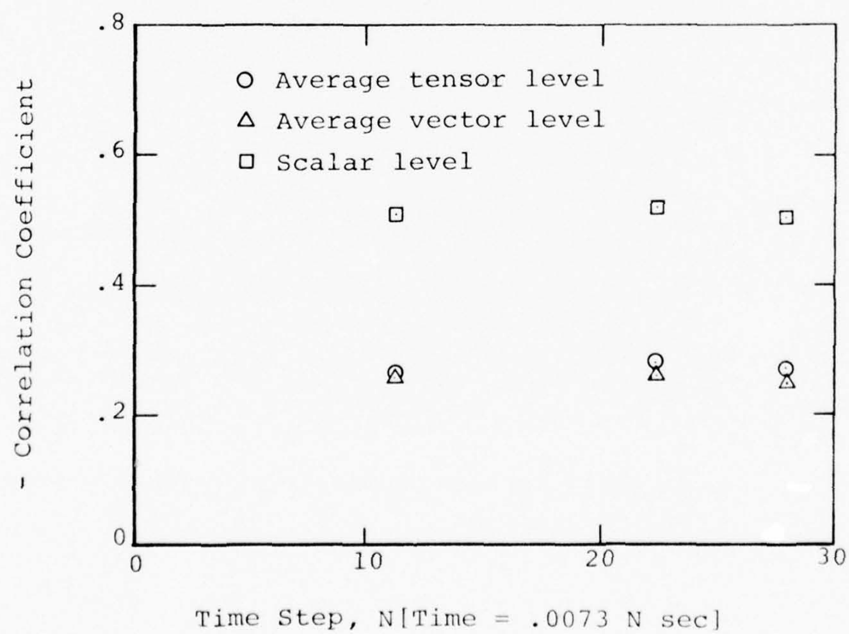

Figure 8. Time development of correlation coefficients and model constants, Smagorinsky model, standard centered differences used in model calculations.

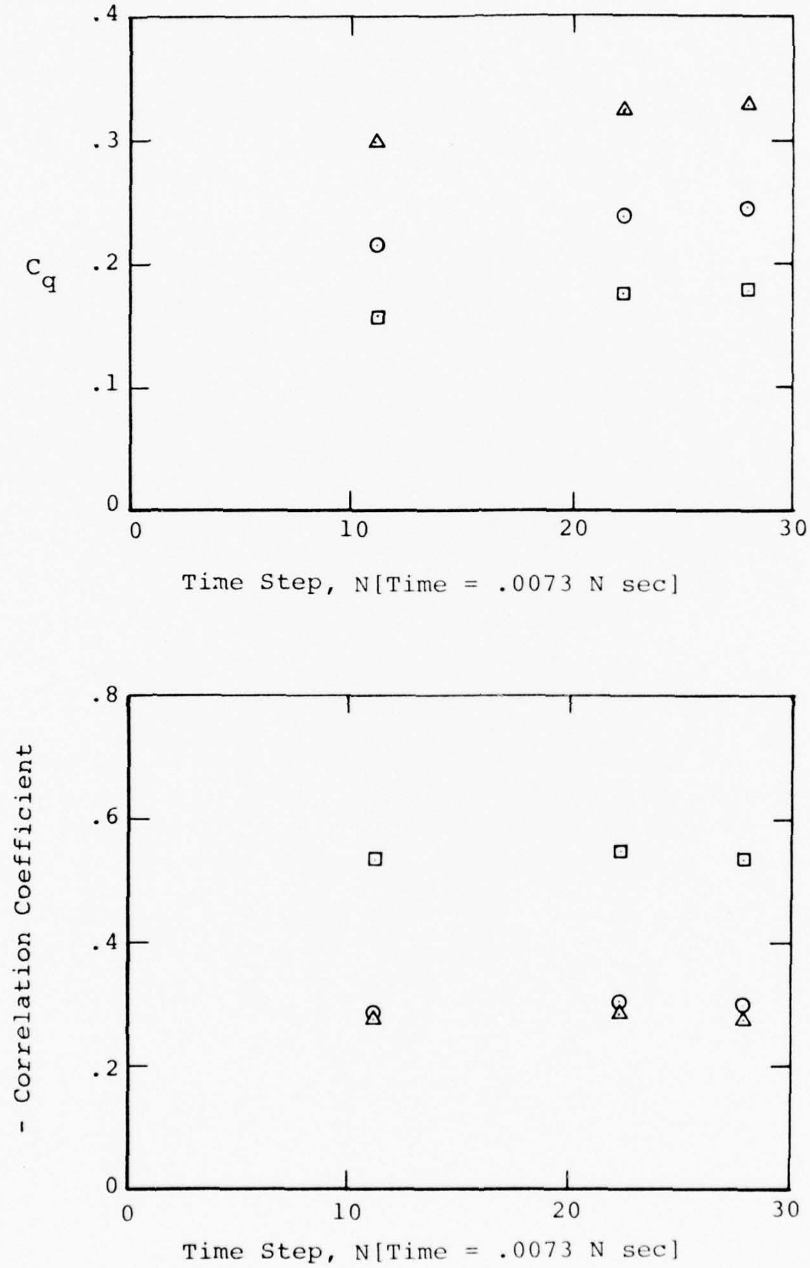

Figure 9. Time development of correlation coefficients and model constants, subgrid-scale kinetic energy model, standard centered differences used in model calculations (for key to symbols, see fig. 8).

TABLE 1. DETAILS OF CORRELATIONS, SMAGORINSKY MODEL, TIME STEP 22.4, STANDARD CENTERED DIFFERENCES USED IN MODEL CALCULATIONS

Tensor Level

i \ j	1	2	3
1	-.358	-.345	-.206
2	-.345	-.288	-.245
3	-.206	-.245	-.285

Average = -.280

Vector Level

i =	1	2	3
	-.259	-.276	-.239

Average = -.258

Scalar Level

-.516

TABLE 2. DETAILS OF CORRELATIONS, VORTICITY MODEL, TIME STEP 22.4, STANDARD CENTERED DIFFERENCES USED IN MODEL CALCULATIONS

Tensor Level

	j = 1	2	3
i = 1	-.326	-.360	-.200
2	-.360	-.258	-.228
3	-.200	-.228	-.260

Average = -.269

Vector Level

i =	1	2	3
	-.267	-.272	-.247

Average -.262

Scalar Level

-.520

TABLE 3. DETAILS OF CORRELATIONS, SUBGRID-SCALE KINETIC ENERGY MODEL, TIME STEP 22.4, STANDARD CENTERED DIFFERENCES USED IN MODEL CALCULATIONS

Tensor Level

	j = 1	2	3
i = 1	-.379	-.380	-.230
2	-.380	-.319	-.262
3	-.230	-.262	-.306

Average = -.305

Vector Level

i =	1	2	3
	-.285	-.304	-.260

Average = -.283

Scalar Level

-.549

TABLE 4. DETAILS OF CORRELATIONS, CONSTANT-EDDY-VISCOSITY MODEL, TIME STEP 22.4, STANDARD CENTERED DIFFERENCES USED IN MODEL CALCULATIONS

Tensor Level

	j = 1	2	3
i = 1	-.358	-.362	-.226
2	-.362	-.301	-.256
3	-.226	-.256	-.290

Average = -.293

Vector Level

i =	1	2	3
	-.270	-.297	-.251

Average = -.273

Scalar Level

-.533

TABLE 5. DETAILS OF MODEL CONSTANTS, TIME STEP 22.4, STANDARD CENTERED DIFFERENCES USED IN MODEL CALCULATIONS

	Model		
Tensor Level	Smagorinsky	Vorticity	Subgrid-scale kinetic energy
Constant for diagonal elements	.160	.177	.229
Constant for off-diagonal elements	.167	.183	.245
Constant for all elements	.164	.180	.238
Vector Level			
Constant for i = 1	.189	.209	.320
Constant for i = 2	.193	.212	.324
Constant for i = 3	.193	.213	.327
Overall constant	.191	.211	.324
Scalar Level			
Constant	.142	.155	.175

TABLE 6. DEPENDENCE OF AVERAGE CORRELATION COEFFICIENTS ON METHOD OF CALCULATING DERIVATIVES IN MODELS, TIME STEP 22.4

	Average Correlation Coefficients			
	Centered Difference Formula (see sketch below)		Spectral Method	Results of Clark (ref. 1)
	L = 1	L = 2		
Tensor Level				
Smagorinsky	-.280	-.161	-.278	-.277
Vorticity	-.269	-.187	-.265	-.260
Kinetic Energy	-.305	-.214	-.299	-.303
Constant κ	-.293	-.202	-.288	-.295
Vector Level				
Smagorinsky	-.258	-.194	-.241	-.346
Vorticity	-.262	-.214	-.245	-.327
Kinetic Energy	-.283	-.230	-.269	-.362
Constant κ	-.273	-.227	-.260	-.356
Scalar Level				
Smagorinsky	-.516	-.474	-.492	-.580
Vorticity	-.520	-.496	-.496	-.582
Kinetic Energy	-.549	-.506	-.537	-.606
Constant κ	-.533	-.502	-.523	-.605

$$\frac{\partial f(I)}{\partial x} \simeq \frac{f(I+L) - f(I-L)}{2(L)(\Delta x)}$$

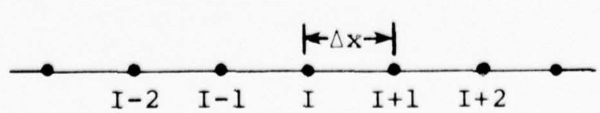

Centered Difference Formula

TABLE 7. SUMMARY OF PARAMETERS AND METHODS OF PRESENT WORK AND THOSE OF CLARK (REF. 1)

	Clark (ref. 1)	Present Work
Navier-Stokes Solution		
Grid (Spacing = Δ)	64^3	64^3
Space Differencing	fourth-order finite difference	spectral
Time Differencing	third-order predictor-corrector	fourth-order Runge-Kutta
Initial Energy Spectrum	from ref. 3	same as Clark's
$(R_\lambda)_{initial}$	38.1	22.3
Filtered Fields		
Grid	8^3	16^3
Filter	Box	Gaussian
Filtering length scale (Δ_a)	8Δ	8Δ
Model Derivatives	fourth-order finite difference	variable (see text)

TABLE 8. DEPENDENCE OF MODEL CONSTANTS ON METHOD OF CALCULATING DERIVATIVES IN MODEL, TIME STEP 22.4

	Model Constant (Tensor and Vector values obtained using all elements)		
	Standard Centered Difference Formula	Spectral Method	Results of Clark (ref. 1)
Tensor Level			
Smagorinsky	.164	.128	.247
Vorticity	.180	.141	.275
Kinetic Energy	.238	.186	.175
Vector Level			
Smagorinsky	.191	.119	.264
Vorticity	.211	.130	.247
Kinetic Energy	.324	.163	.155
Scalar Level			
Smagorinsky	.142	.094	.171
Vorticity	.155	.102	.191
Kinetic Energy	.175	.100	.095

TABLE 9. COMPARISON OF RESULTS OBTAINED BY APPLYING SAME MODELS TO $\tau_{ij} + C_{ij}$ AND TO τ_{ij}, TIME STEP 22.4, STANDARD CENTERED DIFFERENCES USED IN MODEL CALCULATIONS

	Modeled Quantity: $\overline{u_i'u_j'}$		$\overline{u_i'u_j'} + \overline{\bar{u}_i u_j'} + \overline{u_i'\bar{u}_j}$	
Tensor Level	Average Correlation Coefficient	Model Constant	Average Correlation Coefficient	Model Constant
Smagorinsky	-.280	.164	-.198	.301
Vorticity	-.269	.180	-.190	.332
Kinetic Energy	-.305	.238	-.210	.806
Constant K	-.293	----	-.201	----
Vector Level				
Smagorinsky	-.258	.191	-.178	.333
Vorticity	-.262	.211	-.187	.368
Kinetic Energy	-.283	.324	-.194	.980
Constant K	-.273	----	-.187	----
Scalar Level				
Smagorinsky	-.516	.142	-.483	.216
Vorticity	-.520	.155	-.493	.236
Kinetic Energy	-.549	.175	-.514	.404
Constant K	-.533	----	-.499	----

REFERENCES

1. Clark, R. A., Ferziger, J. H. and Reynolds, W. C.: Evaluation of Subgrid-Scale Turbulence Models Using a Fully Simulated Turbulent Flow. Dept. of Mech. Eng., Report No. TF-9, Stanford University, Stanford, CA, March 1977.

2. Rogallo, R. S.: An ILLIAC Program for the Numerical Simulation of Homogeneous Incompressible Turbulence, NASA/Ames Research Center report to be published.

3. Comte-Bellot, G. and Corrsin, S.: Simple Eulerian Time Correlation of Field- and Narrow-Band Velocity Signals in Grid-Generated Isotropic Turbulence. J. Fluid Mech., Vol. 48, part 2, 1971, pp. 273-337.

4. Ferziger, J. H., Mehta, U. B., and Reynolds, W. C.: Large Eddy Simulation of Homogeneous Isotropic Turbulence. Proceedings, Symposium on Turbulent Shear Flows, The Pennsylvania State University, University Park, PA, April 18-20, 1977.

5. Love, M. D. and Leslie, D. C.: Studies of Sub-grid Modeling with Classical Closures and Burgers' Equation. Proceedings, Symposium on Turbulent Shear Flows, The Pennsylvania State University, University Park, PA, April 18-20, 1977.

6. Brigham, E. O.: The Fast Fourier Transform. Prentice Hall, Englewood Cliffs, NJ, 1974, p. 118.

APPENDIX A

SUBPROGRAM AND MAJOR SUBROUTINES IN THE NEAR COMPUTER CODE

CONVERT

Before embarking on the calculations described earlier, the tape generated on the ILLIAC (64 bits/word) must be converted (on the CDC 7600) to the CDC 7600 word structure (60 bits/word) and separate permanent files set up on a private disc pack for the three velocity components u_i. These steps are achieved in program CONVERT. The three files for u_i each contain 64^3 (262,144) words.* A "header" file of global quantities calculated by the ILLIAC is printed out. The velocity components u_i are in the dimensionless form computed on the ILLIAC (the normalization is described in ref. 2).

MAIN

This is the driver program for the CALC series of subprograms. In this program, certain initializations are performed, a back-up copy of the current version of file LCMDAT (described below) is created, three scratch files are created on a disc each with the capacity for a complex 64^3 field (524,288 words), and control is passed to the appropriate CALC subprogram. When the selected CALC has returned control to MAIN, transfer of the results of that CALC to a new version of file LCMDAT is accomplished. In the event of system failure during any CALC, the back-up copy of LCMDAT can be used to restart that CALC.

CALCIA

Permanent files on the private disc pack are set up to later accommodate $\bar{u}_i$, u_i' and $-u_k'u_k'/3$. Each of these files is 64^3 words long. File LCMDAT is also established on the private disc for

*The file lengths quoted are actually slightly larger in practice by the small amount required for system overhead (i.e., index arrays).

later use. This file holds values on the 16^3 mesh of $\partial\tau_{ij}/\partial x_j$, $\bar{u}_i$, $\overline{u'_k u'_k}$ and the 6 independent components of τ_{ij} and is thus 13×16^3 = 53,248 words long.

In this CALC, $\bar{u}_1$, u'_1 and the skewness and flatness for u_1 and $\bar{u}_1$ (S_1, $\bar{S}_1$, F_1, $\bar{F}_1$) are calculated. These quantities are defined as follows:

$$\left.\begin{aligned} S_i &= - \left\langle \left(\frac{\partial u_i}{\partial x_i}\right)^3 \right\rangle \Big/ \left\langle \left(\frac{\partial u_i}{\partial x_i}\right)^2 \right\rangle^{3/2} , \quad \bar{S}_i = - \left\langle \left(\frac{\partial \bar{u}_i}{\partial x_i}\right)^3 \right\rangle \Big/ \left\langle \left(\frac{\partial \bar{u}_i}{\partial x_i}\right)^2 \right\rangle^{3/2} \\ F_i &= - \left\langle \left(\frac{\partial u_i}{\partial x_i}\right)^4 \right\rangle \Big/ \left\langle \left(\frac{\partial u_i}{\partial x_i}\right)^2 \right\rangle^{2} , \quad \bar{F}_i = - \left\langle \left(\frac{\partial \bar{u}_i}{\partial x_i}\right)^4 \right\rangle \Big/ \left\langle \left(\frac{\partial \bar{u}_i}{\partial x_i}\right)^2 \right\rangle^{2} \end{aligned}\right\} \quad \text{(A.1)}$$

In these definitions, the summation convention is suppressed and $\langle\ \rangle$ denotes averaging over the 64^3 field. The skewness and flatness values are printed out, $\bar{u}_1$ and u'_1 are stored in the 64^3 files, and appropriate elements of $\bar{u}_1$ are stored in LCMDAT.

The convolution to calculate the filtered field as expressed in eqn. (2) in the body of this report is done using a system-provided Fast Fourier Transform (FFT) and the discrete convolution theorem (ref. 6). The required multiplication in wave space is done in subroutine FILTER. Differentiation is also done using spectral methods in subroutine DIFFER.

The calculations in CALCIA (and the other CALC's) are done in dimensionless variables. Throughout this series of programs, velocities remain as normalized by Rogallo, and space variables are normalized using Δ, the grid spacing of the 64^3 grid, as the characteristic length.

Operational requirements of the CDC 7600 dictate that the calculations in all CALC's be done in a single x-y or x-z plane (64^2 elements). Further, the FFT can only be invoked with respect to the dimensions present in the plane currently in core (i.e., if an x-y plane is in core, only the x and y transforms of that plane can be taken). Thus, multiple passes through the data files are required. Input-output routines GETPL, GETRPL, PUTPL, and PUTRPL do most of the required data transfer.

CALCIB

In a similar fashion to that described in CALCIA, $\bar{u}_2$, u_2' and S_2, $\bar{S}_2$, F_2, $\bar{F}_2$ are calculated. The skewness and flatness values are printed out, $\bar{u}_2$ and u_2' are stored in 64^3 files, and appropriate elements of $\bar{u}_2$ are stored in LCMDAT.

CALCIC

As above, $\bar{u}_3$, u_3', S_3, $\bar{S}_3$, F_3, $\bar{F}_3$ are calculated and stored or printed out.

CALCII

Values of $\overline{u_1'u_2'}$, $\partial\overline{u_1'u_2'}/\partial x_1$, and $\partial\overline{u_1'u_2'}/\partial x_2$ are calculated on the 64^3 grid. Appropriate elements (on the 16^3 grid) are stored as τ_{12} and as partial values of $\partial\tau_{2j}/\partial x_j$ and $\partial\tau_{1j}/\partial x_j$, respectively, in LCMDAT.

CALCIII

Values of $\overline{u_1'u_3'}$, $\partial\overline{u_1'u_3'}/\partial x_1$, and $\partial\overline{u_1'u_3'}/\partial x_3$ are calculated on the 64^3 grid. In LCMDAT, $\overline{u_1'u_3'}$ is stored as τ_{13}, $\partial\tau_{13}/\partial x_1$ is stored as a partial value of $\partial\tau_{3j}/\partial x_j$, and $\partial\tau_{13}/\partial x_3$ is added to the previous partial value of $\partial\tau_{1j}/\partial x_j$.

CALCIV

Values of $\overline{u_2'u_3'}$, $\partial\overline{u_2'u_3'}/\partial x_2$, and $\partial\overline{u_2'u_3'}/\partial x_3$ are calculated on the 64^3 grid. In LCMDAT, $\overline{u_2'u_3'}$ is stored as τ_{23}, $\partial\tau_{23}/\partial x_2$ is added to $\partial\tau_{3j}/\partial x_j$, and $\partial\tau_{23}/\partial x_3$ is added to $\partial\tau_{2j}/\partial x_j$.

CALCV

On the 64^3 grid, $-1/3\ u_k'u_k'$, $\overline{u_k'u_k'}$, $\overline{u_1'^2} - 1/3\ \overline{u_k'u_k'} = \tau_{11}$, and $\partial\tau_{11}/\partial x_1$ are calculated. The first field is stored in the file defined for it in CALCIA. In LCMDAT, τ_{11} and $\overline{u_k'u_k'}$ are stored, and $\partial\tau_{11}/\partial x_1$, is added to $\partial\tau_{1j}/\partial x_j$.

CALCVI

On the 64^3 grid, $\overline{u_2'^2} - 1/3\ \overline{u_k'u_k'} = \tau_{22}$ and $\partial\tau_{22}/\partial x_2$ are calculated. In LCMDAT, τ_{22} is stored and $\partial\tau_{22}/\partial x_2$ is added to $\partial\tau_{2j}/\partial x_j$.

CALCVII

On the 64^3 grid, $\overline{u_3'^2} - 1/3\ \overline{u_k'u_k'} = \tau_{33}$ and $\partial\tau_{33}/\partial x_3$ are calculated. In LCMDAT, τ_{33} is stored and $\partial\tau_{33}/\partial x_3$ is added to $\partial\tau_{3j}/\partial x_j$.

INCORE

LCMDAT is the input to this subprogram which operates only on data on the 16^3 grid. The correlation coefficients and model constants discussed earlier are calculated. The derivatives required in the model calculations, for example to calculate $\bar{S}_{ij}$ or $\partial M_{ij}/\partial x_j$, are done by the spectral method, by a standard centered difference scheme (L = 1 in the sketch below), or by a modified central difference scheme with L > 1.

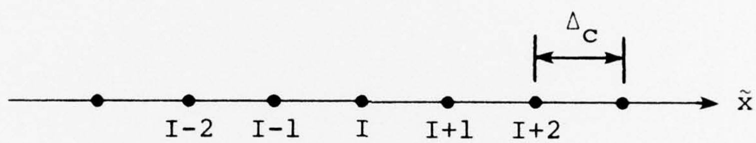

$$\left.\begin{aligned} &\text{Dimensional:} && \left.\frac{\partial \tilde{f}}{\partial \tilde{x}}\right)_I \simeq \frac{\tilde{f}(I+L) - \tilde{f}(I-L)}{2(L)\Delta_c} \\ &\text{Dimensionless:} && \left.\frac{\partial f}{\partial x}\right)_I \simeq \frac{f(I+L) - f(I-L)}{2(L)\Delta_c/\Delta} \end{aligned}\right\} \tag{A.2}$$

Δ_c is the grid spacing on the coarse (16^3) mesh ($\Delta_c/\Delta = 4$)

FILTER

This subroutine does the multiplication in wave space corresponding to a convolution in physical space. It forms the product

$$\hat{\hat{f}}(i,j) = \hat{f}(i,j)\ g_1(i)\ g_2(j)\ g_3(k)/64^3 \tag{A.3}$$

on the kth x-y wave number plane, or the product

$$\hat{\hat{f}}(i,k) = \hat{f}(i,k)\ g_1(i)\ g_2(j)\ g_3(k)/64^3 \tag{A.4}$$

on the jth x-z wave number plane, where i,j,k are the indices in the x,y,z wave number directions, respectively, ($\hat{\ }$) denotes a three-dimensionally Fourier transformed variable, and g_1, g_2, g_3

are the one-dimensional Fourier transforms of the components of the filter function, $G_i(\underline{x})$, where

$$G(\underline{x}) = G_1(x_1)\ G_2(x_2)\ G_3(x_3)\ . \tag{A.5}$$

This construction allows for the possibility of a nonisotropic filter. g_1, g_2, and g_3 are generated in subroutine GHATGEN.

GHATGEN

This subroutine forms the one-dimensional Fourier transforms of the filter function components. The filter function implemented at this time is a three-dimensional Gaussian:

$$G(\underline{x}) = \left(\sqrt{6/\pi}\ \frac{1}{\Delta_a/\Delta}\right)^3 \exp\left[-\ \frac{6}{(\Delta_a/\Delta)^2}\ (x_1^2 + x_2^2 + x_3^2)\right] \tag{A.6}$$

This filter is isotropic with a filtering length scale of Δ_a. The value of Δ_a/Δ is taken to be 8, implying that $\Delta_a/\Delta_c = 2$. The set g_i is the set of discretized continuous one-dimensional Fourier transforms of this filter function:

$$\left.\begin{aligned} g_1(i) &= \exp\left[-\ \frac{(\Delta_a/\Delta)^2}{6}\ \left(\frac{\pi i}{64}\right)^2\right] \\ g_2(j) &= \exp\left[-\ \frac{(\Delta_a/\Delta)^2}{6}\ \left(\frac{\pi j}{64}\right)^2\right] \\ g_3(k) &= \exp\left[-\ \frac{(\Delta_a/\Delta)^2}{6}\ \left(\frac{\pi k}{64}\right)^2\right] \end{aligned}\right\} \tag{A.7}$$

In general, the functions g_i are constrained to be real, which implies that the filter function must be even.

DIFFER

This subroutine performs the multiplication in wave space corresponding to differentiation in physical space. It forms the product

$$\widehat{\frac{\partial f}{\partial x}}(i,j) = \sqrt{-1}\left(\frac{2\pi i}{64}\right)\hat{f}(i,j) \text{ or } \widehat{\frac{\partial f}{\partial y}}(i,j) = \sqrt{-1}\,\frac{2\pi j}{64}\,\hat{f}(i,j) \qquad (A.8)$$

in an x-y wave number plane,

$$\widehat{\frac{\partial f}{\partial x}}(i,k) = \sqrt{-1}\left(\frac{2\pi i}{64}\right)\hat{f}(i,k) \text{ or } \widehat{\frac{\partial f}{\partial z}}(i,k) = \sqrt{-1}\,\frac{2\pi k}{64}\,\hat{f}(i,k) \qquad (A.9)$$

in an x-z wave number plane. Note that the indicated multiplications are complex.

GETPL and PUTPL

These subroutines are input and output subroutines, respectively, which move planes of complex elements between small core memory and disc storage using random access methods. The file and array names involved and the plane number are arguments in the call. The plane can be either an x-y plane or an x-z plane.

GETRPL and PUTRPL

These subroutines are input and output subroutines, respectively, which move plane of elements between small core memory and disc storage, just as above. The difference is that for GETRPL and PUTRPL the elements in mass storage are real, while the array in core may be complex. On input, this means that the imaginary part of the array is set to 0; on output, the imaginary part is lost.

LIST OF SYMBOLS

C_c	constant in constant-eddy-viscosity model
C_q	constant in subgrid-scale kinetic-energy model
C_s	constant in Smagorinsky model
C_v	constant in vorticity model
C_{ij}	cross-scale stress, eqn. (3)
E	three-dimensional energy spectrum, cm^3/sec^2
F_i	velocity-gradient flatness, eqn. (A.1)
$\bar{F}_i$	velocity-gradient flatness for filtered field, eqn. (A.1)
f	any field variable
$G(\underline{x})$	spatial filter function
$G_i(x_i)$	component of spatial filter function, eqn. (A.5)
g_i	one-dimensional Fourier transform of $G_i(x_i)$, eqn. (A.7)
i,j,k	indices in x, y, and z wave number directions
K	eddy viscosity
k	shell wave number, cm^{-1}
L	spacing variable in centered difference formula, eqn. (A.2)
M_{ij}	subgrid-scale stress model, $M_{ij} = \alpha_{ij} - \frac{1}{3}\alpha_{kk}\delta_{ij}$
P	reduced pressure, eqn. (3)
p	pressure
R_λ	Reynolds number based on Taylor microscale
$\bar{S}_{ij}$	rate of strain tensor for filtered field, $\bar{S}_{ij} = \frac{1}{2}\left(\frac{\partial \bar{u}_i}{\partial x_j} + \frac{\partial \bar{u}_j}{\partial x_i}\right)$
S_i	velocity-gradient skewness, eqn. (A.1)
$\bar{S}_i$	velocity-gradient skewness for filtered field, eqn. (A.1)
t	time
u_i	velocity

LIST OF SYMBOLS (concluded)

$\bar{u}_i$	filtered velocity
u_i'	subgrid-scale velocity, eqn. (3)
x_i	spatial coordinate
α_{ij}	$\alpha_{ij} = 2K\bar{S}_{ij}$
Δ	grid spacing for 64^3 grid
Δ_c	grid spacing for coarse grid
Δ_a	length scale for filter function
ε_τ	subgrid-scale dissipation, $\varepsilon_\tau = \frac{1}{N^3} \sum^{N^3} \bar{u}_i \frac{\partial \tau_{ij}}{\partial x_j}$ N = number of grid points in coarse grid
ν	kinematic viscosity
ρ	density
τ_{ij}	subgrid-scale stress, eqn. (3)
ω_i	vorticity

Subscripts

1,2,3 i,j,k	coordinate directions
$-$	vector quantity

Superscripts

$-$	filtered variable, eqn. (2)
'	subgrid-scale variable
~	dimensional variable in the Appendix
^	three-dimensionally Fourier transformed variable

DISTRIBUTION LIST FOR UNCLASSIFIED
TECHNICAL REPORTS AND REPRINTS ISSUED UNDER
CONTRACT N00014-77-C-0008 TASK NR 061-244

All addresses receive one copy unless otherwise specified

Technical Library
Building 313
Ballistic Research Laboratories
Aberdeen Proving Ground, MD 21005

Dr. F. D. Bennett
External Ballistic Laboratory
Ballistic Research Laboratories
Aberdeen Proving Ground, MD 21005

Mr. C. C. Hudson
Sandia Corporation
Sandia Base
Albuquerque, NM 81115

Professor P. J. Roache
Ecodynamics Research
Associates, Inc.
P. O. Box 8172
Albuquerque, NM 87108

Dr. J. D. Shreve, Jr.
Sandia Corporation
Sandia Base
Albuquerque, NM 81115

Defense Documentation Center
Cameron Station, Building 5
Alexandria, VA 22314 12 Copies

Library
Naval Academy
Annapolis, MD 21402

Dr. G. H. Heilmeier
Director, Defense Advanced
Research Projects Agency
1400 Wilson Boulevard
Arlington, VA 22209

Mr. R. A. Moore
Deputy Director, Tactical
Technology Office
Defense Advanced Research Projects
Agency
1400 Wilson Boulevard
Arlington, VA 22209

Office of Naval Research
Code 411
Arlington, VA 22217

Office of Naval Research
Code 421
Arlington, VA 22217

Office of Naval Research
Code 438
Arlington, VA 22217

Office of Naval Research
Code 1021P (ONRL)
Arlington, VA 22217 6 Copies

Dr. J. L. Potter
Deputy Director, Technology
von Karman Gas Dynamics Facility
Arnold Air Force Station, TN 37389

Professor J. C. Wu
Georgia Institute of Technology
School of Aerospace Engineering
Atlanta, GA 30332

Library
Aerojet-General Corporation
6352 North Irwindale Avenue
Azusa, CA 91702

NASA Scientific and Technical
Information Facility
P. O. Box 8757
Baltimore/Washington International Airport
Maryland 21240

Dr. S. A. Berger
University of California
Department of Mechanical Engineering
Berkeley, CA 94720

Professor A. J. Chorin
University of California
Department of Mathematics
Berkeley, CA 94720

Professor M. Holt
University of California
Department of Mechanical Engineering
Berkeley, CA 94720

Dr. L. Talbot
University of California
Department of Mechanical Engineering
Berkeley, CA 94720

Dr. H. R. Chaplin
Code 16
David W. Taylor Naval Ship Research
and Development Center
Bethesda, MD 20084

Code 1800
David W. Taylor Naval Ship Research
and Development Center
Bethesda, MD 20084

Code 5643
David W. Taylor Naval Ship Research
and Development Center
Bethesda, MD 20084

Dr. G. R. Inger
Virginia Polytechnic Institute
and State University
Department of Aerospace Engineering
Blacksburg, VA 24061

Professor A. H. Nayfeh
Virginia Polytechnic Institute
and State University
Department of Engineering Science
and Mechanics
Blacksburg, VA 24061

Indiana University
School of Applied Mathematics
Bloomington, IN 47401

Director
Office of Naval Research Branch Office
495 Summer Street
Boston, MA 02210

Supervisor, Technical Library Section
Thiokol Chemical Corporation
Wasatch Division
Brigham City, UT 84302

Dr. G. Hall
State University of New York at Buffalo
Faculty of Engineering and
Applied Science
Fluid and Thermal Sciences Laboratory
Buffalo, NY 14214

Mr. R. J. Vidal
Calspan Corporation
Aerodynamics Research Department
P. O. Box 235
Buffalo, NY 14221

Professor R. F. Probstein
Massachusetts Institute of Technology
Department of Mechanical Engineering
Cambridge, MA 02139

Director
Office of Naval Research Branch Office
536 South Clark Street
Chicago, IL 60605

Code 753
Naval Weapons Center
China Lake, CA 93555

Mr. J. Marshall
Code 4063
Naval Weapons Center
China Lake, CA 93555

Professor R. T. Davis
University of Cincinnati
Department of Aerospace Engineering
and Applied Mechanics
Cincinnati, OH 45221

Library MS 60-3
NASA Lewis Research Center
21000 Brookpark Road
Cleveland, OH 44135

Dr. J. D. Anderson, Jr.
Chairman, Department of Aerospace
Engineering
College of Engineering
University of Maryland
College Park, MD 20742

Professor W. L. Melnik
University of Maryland
Department of Aerospace Engineering
Glenn L. Martin Institute of Technology
College Park, MD 20742

Professor O. Burggraf
Ohio State University
Department of Aeronautical and
Astronautical Engineering
1314 Kinnear Road
Columbus, OH 43212

Technical Library
Naval Surface Weapons Center
Dahlgren Laboratory
Dahlgren, VA 22448

Dr. F. Moore
Naval Surface Weapons Center
Dahlgren Laboratory
Dahlgren, VA 22448

Technical Library 2-51131
LTV Aerospace Corporation
P. O. Box 5907
Dallas, TX 75222

Library, United Aircraft Corporation
Research Laboratories
Silver Lane
East Hartford, CT 06108

Technical Library
AVCO-Everett Research Laboratory
2385 Revere Beach Parkway
Everett, MA 02149

Professor G. Moretti
Polytechnic Institute of New York
Long Island Center
Department of Aerospace Engineering
and Applied Mechanics
Route 110
Farmingdale, NY 11735

Professor S. G. Rubin
Polytechnic Institute of New York
Long Island Center
Department of Aerospace Engineering
and Applied Mechanics
Route 110
Farmingdale, NY 11735

Technical Documents Center
Army Mobility Equipment R&D Center
Building 315
Fort Belvoir, VA 22060

Dr. W. R. Briley
Scientific Research Associates, Inc.
P. O. Box 498
Glastonbury, CT 06033

Library (MS 185)
NASA Langley Research Center
Langley Station
Hampton, VA 23665

Dr. S. Nadir
Northrop Corporation
Aircraft Division
3901 West Broadway
Hawthorne, CA 90250

Professor A. Chapmann
Chairman, Mechanical Engineering
Department
William M. Rice Institute
Box 1892
Houston, TX 77001

Dr. F. Lane
KLD Associates, Inc.
300 Broadway
Huntington Station, NY 11746

Technical Library
Naval Ordnance Station
Indian Head, MD 20640

Professor D. A. Caughey
Cornell University
Sibley School of Mechanical and
Aerospace Engineering
Ithaca, NY 14853

Professor E. L. Resler
Cornell University
Sibley School of Mechanical and
Aerospace Engineering
Ithaca, NY 14853

Professor S. F. Shen
Cornell University
Sibley School of Mechanical and
Aerospace Engineering
Ithaca, NY 14853

Library
Midwest Research Institute
425 Volker Boulevard
Kansas City, MO 64110

Dr. M. M. Hafez
Flow Research, Inc.
P. O. Box 5040
Kent, WA 98031

Dr. E. M. Murman
Flow Research, Inc.
P. O. Box 5040
Kent, WA 98031

Dr. S. A. Orszag
Cambridge Hydrodynamics, Inc.
54 Baskin Road
Lexington, MA 02173

Professor T. Cebeci
California State University, Long Beach
Mechanical Engineering Department
Long Beach, CA 90840

Mr. J. L. Hess
Douglas Aircraft Company
3855 Lakewood Boulevard
Long Beach, CA 90808

Dr. H. K. Cheng
University of Southern California, University Park
Department of Aerospace Engineering
Los Angeles, CA 90007

Professor J. D. Cole
University of California
Mechanics and Structures Department
School of Engineering and Applied Science
Los Angeles, CA 90024

Engineering Library
University of Southern California
Box 77929
Los Angeles, CA 90007

Dr. C. -M. Ho
University of Southern California, University Park
Department of Aerospace Engineering
Los Angeles, CA 90007

Dr. T. D. Taylor
The Aerospace Corporation
P. O. Box 92957
Los Angeles, CA 90009

Commanding Officer
Naval Ordnance Station
Louisville, KY 40214

Mr. B. H. Little, Jr.
Lockheed-Georgia Company
Department 72-74, Zone 369
Marietta, GA 30061

Dr. C. Cook
Stanford Research Institute
Menlo Park, CA 94025

Professor E. R. G. Eckert
University of Minnesota
241 Mechanical Engineering Building
Minneapolis, MN 55455

Library
Naval Postgraduate School
Monterey, CA 93940

McGill University
Supersonic-Gas Dynamics Research Laboratory
Department of Mechanical Engineering
Montreal 12, Quebec, Canada

Librarian
Engineering Library, 127-223
Radio Corporation of America
Morristown, NJ 07960

Dr. S. S. Stahara
Nielsen Engineering & Research, Inc.
510 Clyde Avenue
Mountain View, CA 94043

Engineering Societies Library
345 East 47th Street
New York, NY 10017

Professor A. Jameson
New York University
Courant Institute of Mathematical Sciences
251 Mercer Street
New York, NY 10012

Professor G. Miller
New York University
Department of Applied Science
26-36 Stuyvesant Street
New York, NY 10003

Office of Naval Research
New York Area Office
715 Broadway - 5th Floor
New York, NY 10003

Dr. A. Vaglio-Laurin
New York University
Department of Applied Science
26-36 Stuyvesant Street
New York, NY 10003

Professor S. Weinbaum
Research Foundation of the City
University of New York on behalf
of the City College
1411 Broadway
New York, NY 10018

Librarian, Aeronautical Library
National Research Council
Montreal Road
Ottawa 7, Canada

Lockheed Missiles and Space Company
Technical Information Center
3251 Hanover Street
Palo Alto, CA 94304

Director
Office of Naval Research Branch Office
1030 East Green Street
Pasadena, CA 91106

California Institute of Technology
Engineering Division
Pasadena, CA 91109

Library
Jet Propulsion Laboratory
4800 Oak Grove Drive
Pasadena, CA 91103

Professor H. Liepmann
California Institute of Technology
Department of Aeronautics
Pasadena, CA 91109

Mr. L. I. Chasen, MGR-MSD Lib.
General Electric Company
Missile and Space Division
P. O. Box 8555
Philadelphia, PA 19101

Mr. P. Dodge
Airesearch Manufacturing Company
of Arizona
Division of Garrett Corporation
402 South 36th Street
Phoenix, AZ 85034

Technical Library
Naval Missile Center
Point Mugu, CA 93042

Professor S. Bogdonoff
Princeton University
Gas Dynamics Laboratory
Department of Aerospace and
Mechanical Sciences
Princeton, NJ 08540

Professor S. I. Cheng
Princeton University
Department of Aerospace and
Mechanical Sciences
Princeton, NJ 08540

Dr. J. E. Yates
Aeronautical Research Associates
of Princeton, Inc.
50 Washington Road
Princeton, NJ 08540

Professor J. H. Clarke
Brown University
Division of Engineering
Providence, RI 02912

Professor J. T. C. Liu
Brown University
Division of Engineering
Providence, RI 02912

Professor L. Sirovich
Brown University
Division of Applied Mathematics
Providence, RI 02912

Dr. P. K. Dai (R1/2178)
TRW Systems Group, Inc.
One Space Park
Redondo Beach, CA 90278

Redstone Scientific Information Center
Chief, Document Section
Army Missile Command
Redstone Arsenal, AL 35809

U.S. Army Research Office
P. O. Box 12211
Research Triangle, NC 27709

Professor M. Lessen
The University of Rochester
Department of Mechanical Engineering
River Campus Station
Rochester, NY 14627

Editor, Applied Mechanics Review
Southwest Research Institute
8500 Culebra Road
San Antonio, TX 78228

Library and Information Services
General Dynamics-CONVAIR
P. O. Box 1128
San Diego, CA 92112

Dr. R. Magnus
General Dynamics-CONVAIR
Kearny Mesa Plant
P. O. Box 80847
San Diego, CA 92138

Mr. T. Brundage
Defense Advanced Research Projects Agency
Research and Development Field Unit
APO 146, Box 271
San Francisco, CA 96246

Office of Naval Research
San Francisco Area Office
760 Market Street - Room 447
San Francisco, CA 94102

Library
The Rand Corporation
1700 Main Street
Santa Monica, CA 90401

Department Librarian
University of Washington
Department of Aeronautics and Astronautics
Seattle, WA 98105

Dr. P. E. Rubbert
Boeing Commercial Airplane Company
P. O. Box 3707
Seattle, WA 98124

Mr. R. Feldhuhn
Naval Surface Weapons Center
White Oak Laboratory
Silver Spring, MD 20910

Dr. G. Heiche
Naval Surface Weapons Center
Mathematical Analysis Branch
Silver Spring, MD 20910

Librarian
Naval Surface Weapons Center
White Oak Laboratory
Silver Spring, MD 20910

Dr. J. M. Solomon
Naval Surface Weapons Center
White Oak Laboratory
Silver Spring, MD 20910

Professor J. H. Ferziger
Stanford University
Department of Mechanical Engineering
Stanford, CA 94305

Professor K. Karamcheti
Stanford University
Department of Aeronautics and Astronautics
Stanford, CA 94305

Professor M. van Dyke
Stanford University
Department of Aeronautics and Astronautics
Stanford, CA 94305

Engineering Library
McDonnell Douglas Corporation
Department 218, Building 101
P. O. Box 516
St. Louis, MO 63166

Dr. R. J. Hakkinen
McDonnell Douglas Corporation
Department 222
P. O. Box 516
St. Louis, MO 63166

Dr. R. P. Heinisch
Honeywell, Inc.
Systems and Research Division -
Aerospace Defense Group
2345 Walnut Street
St. Paul, MN 55113

Professor R. G. Stoner
Arizona State University
Department of Physics
Tempe, AZ 85721

Dr. N. Malmuth
Rockwell International
Science Center
1049 Camino Dos Rios
P. O. Box 1085
Thousand Oaks, CA 91360

Rockwell International
Science Center
1049 Camino Dos Rios
P. O. Box 1085
Thousand Oaks, CA 91360

The Library
University of Toronto
Institute of Aerospace Studies
Toronto 5, Canada

Professor W. R. Sears
University of Arizona
Aerospace and Mechanical Engineering
Tucson, AZ 85721

Professor A. R. Seebass
University of Arizona
Department of Aerospace and
Mechanical Engineering
Tucson, AZ 85721

Dr. S. M. Yen
University of Illinois
Coordinated Science Laboratory
Urbana, IL 61801

Dr. K. T. Yen
Code 3015
Naval Air Development Center
Warminster, PA 18974

Air Force Office of Scientific
Research (SREM)
Building 410, Bolling AFB
Washington, DC 20332

Chief of Research & Development
Office of Chief of Staff
Department of the Army
Washington, DC 20310

Library of Congress
Science and Technology Division
Washington, DC 20540

Director of Research (Code RR)
National Aeronautics and
Space Administration
600 Independence Avenue, SW
Washington, DC 20546

Library
National Bureau of Standards
Washington, DC 20234

National Science Foundation
Engineering Division
1800 G Street, NW
Washington, DC 20550

Mr. W. Koven (AIR 03E)
Naval Air Systems Command
Washington, DC 20361

Mr. R. Siewert (AIR 320D)
Naval Air Systems Command
Washington, DC 20361

Technical Library Division (AIR 604)
Naval Air Systems Command
Washington, DC 20361

Code 2627
Naval Research Laboratory
Washington, DC 20375

SEA 03512
Naval Sea Systems Command
Washington, DC 20362

SEA 09G3
Naval Sea Systems Command
Washington, DC 20362

Dr. A. L. Slafkosky
Scientific Advisor
Commandant of the Marine Corps
(Code AX)
Washington, DC 20380

Director
Weapons Systems Evaluation Group
Washington, DC 20305

Dr. P. Baronti
General Applied Science
Laboratories, Inc.
Merrick and Stewart Avenues
Westbury, NY 11590

Bell Laboratories
Whippany Road
Whippany, NJ 07981

Chief of Aerodynamics
AVCO Corporation
Missile Systems Division
201 Lowell Street
Wilmington, MA 01887

Research Library
AVCO Corporation
Missile Systems Division
201 Lowell Street
Wilmington, MA 01887

AFAPL (APRC)
AB
Wright Patterson, AFB, OH 45433

Dr. Donald J. Harney
AFFDL/FX
Wright Patterson AFB, OH 45433